Introduction of Sliding Capabilities in the ICFD LS-DYNA® Solver

Iñaki Çaldichoury[1], Chienjung Huang[1], Facundo Del Pin[1], Rodrigo Paz[1]
[1]Livermore Software Technology, an Ansys company, Livermore, CA, USA

Abstract

Sliding mesh is a technique that prevents excessive re-meshing in problems that involve rotating parts. It is ideal for solving transient problems in turbo-machinery. Overset mesh techniques on the other hand typically contain the body of interest for the study around which a fine fluid mesh in constructed. That initial domain is then superimposed on a background mesh containing the surrounding geometry with data being interpolated between the two. Other techniques include using a non-inertial rotating frame or using immersed FSI techniques.

Within LS-DYNA, the ICFD solver has seen a continuous growth of users that wish to simulate increasingly complex multiphysics problems involving moving structures, thermal heating, particle displacement and sometimes magnetic fields. As such, it is imperative to offer as many advanced CFD capabilities and solving tools to the users as possible. Among those, sliding mesh has been amongst the most prominent requests.

In this paper, the current state of development will be presented, along with a description of the algorithm used as well as some examples and some benchmarking results.

The ICFD Solver: Numerical Methods

The ICFD solver studies the motion of incompressible fluids and their interaction with rigid or flexible solid boundaries in cases of fluid structure interaction. In the case of the ICFD solver the equations of motion are defined by the Navier-Stokes equations and the continuity equation. The numerical scheme used in the approximation of the system is based on the FEM. Furthermore, the discrete model will be decoupled by means of a fractional step method first proposed by Chorin [1] and Temam [2]. Using a backward difference time integration scheme, the following system is obtained:

Predictor step

$$\left(\frac{\rho}{\delta t}\boldsymbol{M} + \mu\boldsymbol{K} + \rho\boldsymbol{S}\left(\boldsymbol{u_k^{n+1}}\right)\right)u_{k+1}^{*} = -\boldsymbol{G}P_k^{n+1} + \frac{\rho}{\delta t}\boldsymbol{M}u^n \tag{1}$$

Poisson equation

$$\boldsymbol{L}P_{k+1}^{n+1} = \frac{\rho}{\delta t}\boldsymbol{D}u_{k+1}^{*} + \boldsymbol{L}P_k^{n+1} \tag{2}$$

where the standard assembled FEM matrices are $\boldsymbol{M}$ for the mass matrix, $\boldsymbol{K}$ is the stiffness matrix, $\boldsymbol{L}$ is the Laplacian matrix, $\boldsymbol{D}$ is the divergence, $\boldsymbol{G}$ is the gradient matrix. The matrix $\boldsymbol{S}$ is the advection matrix which depends on the fluid velocity of the previous iteration or timestep at the beginning of the loop. The variable u^* is an intermediate velocity that is also predicted using the pressure of the previous iteration in its right-hand-side. The sub-index k indicates the iteration sub-step for the prediction corrector step and n indicates the current timestep. The system can be solved for a number of iterations k or until the pressure difference in the Poisson equation vanishes and the divergence free velocity condition is achieved. This can be controlled in the keyword *ICFD_SOLVER_SPLIT. In most practical applications and in the interest of reducing computation costs, a single pass is done on the Predictor step and for the Poisson equation. The resulting pressure is then injected in a final momentum equation solve which acts as de-facto "Corrector Step". Finally, the Orthogonal Subgrid-Scale (OSS) method by Codina [3] is implemented for stabilization purposes.

In order for the system description to be complete, boundary conditions must be introduced. Dirichlet type boundary conditions are typically applied on the velocity and pressure variables to define inlets, outlets and walls. More complex types of constraints can be employed to handle advanced boundary conditions such as periodic or sliding surfaces. Their use will be further discussed in the following sections.

Finally, the velocity system is non-symmetric and is solved with an iterative GMRES method with diagonal preconditioner while the continuity equation forms a symmetric system and is solved with a conjugate gradient method and block diagonal preconditioner with a drop tolerance factorization on each bloc.

Modeling of a wind turbine

The first case of interest here will be the study of a wind turbine rotating with a prescribed angular velocity ramping up linearly for the first 0.2 seconds. The geometry is loosely based on the case described in depth by Bazilevs [4]. Table 1 offers a view of the chosen parameters for this study. No specific care has been conducted in choosing the Center of Torque which has been left at its default position on the wind turbine nose. A LES Smagorinsky turbulence model has been chosen for this study with a simple boundary layer mesh representation. A fixed time step of 5.e-4 seconds is used for all cases.

Inlet Velocity	$9\ m.s^{-1}$
Density	$1.225\ kg.m^{-3}$
Viscosity	$1.87\ kg.m^{-1}s^{-1}$
Rotor Velocity	$1.08\ rad.s^{-1}$

Table 1 Wind turbine input parameters

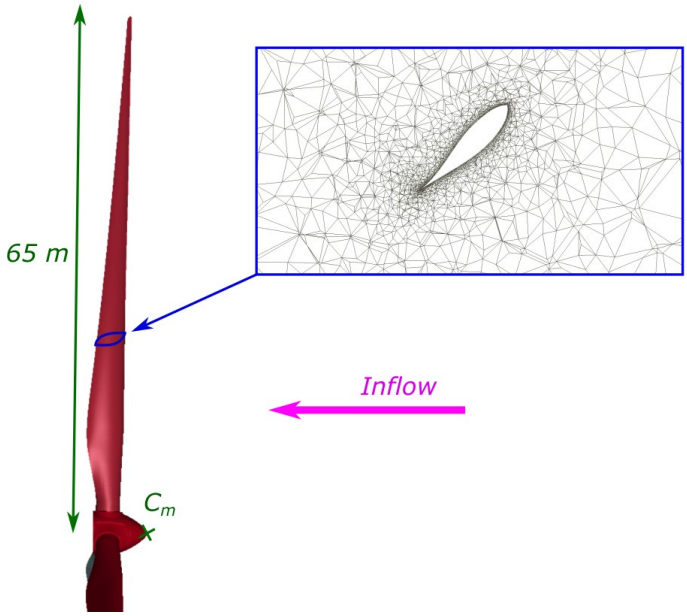

Figure 1 Wind turbine mesh around an airfoil section

Several techniques are available to the user within the ICFD solver. The first method consists in directly imposing a Lagrangian displacement of the surface mesh of the wind turbine. To that effect, the keyword *ICFD_CONTROL_IMPOSED_MOVE may be used and an ALE formulation for the solver is retrieved. The modified system reads:

$$\left(\frac{\rho}{\delta t}\boldsymbol{M} + \mu\boldsymbol{K} + \rho\boldsymbol{S}\left(\boldsymbol{u_k^{n+1}} - \boldsymbol{v_m^n}\right)\right)u_{k+1}^{*} -= -\boldsymbol{G}P_k^{n+1} + \frac{\rho}{\delta t}\boldsymbol{M}u^n \quad (1)$$

$$\boldsymbol{L}\left(\frac{1}{h^n}\right)v_m^{n+1} = 0.$$

With $\boldsymbol{v_m}$ the velocity of the mesh. The Dirichlet wall condition $\boldsymbol{u} = \boldsymbol{0}$ is shifted to $\boldsymbol{u} = \boldsymbol{v_m}$.

Compared to the pure Eulerian formulation, an additional Laplace equation $\boldsymbol{L}\left(\frac{1}{h}\right)$, with h the local element size, is needed to handle the mesh displacement. This bears additional cost to the solver especially in cases involving boundary layer meshes which can hurt the matrix conditioning. Furthermore, in this particular case, the distortion of the mesh would result in an element inversion. To prevent that, a remeshing in necessary. Again, several keywords, *ICFD_CONTROL_ADAPT and *ICFD_CONTROL_ADAPT_SIZE allow the user to choose between different techniques.

In order to avoid this mesh distortion and frequent remeshing, a non-inertial reference frame may be used instead. The modified system for the momentum equation reads:

$$\left(\frac{\rho}{\Delta t}\boldsymbol{M} + \mu\boldsymbol{K} + \rho\boldsymbol{S}\left(\boldsymbol{u_k^{n+1}} - \boldsymbol{v_\Omega}\right)\right)u_{k+1}^{*} -= -\boldsymbol{G}P_k^{n+1} + \frac{\rho}{\Delta t}\boldsymbol{M}u^n + F \quad (1)$$

With F the non-inertial body force expressed as $F = \rho(w_i \times u^n)$, w_i the angular velocity. For all wall nodes belonging to the non-inertial frame, the Dirichlet condition $\boldsymbol{u} = \boldsymbol{0}$. is shifted to $\boldsymbol{u} = \boldsymbol{v_\Omega} = \boldsymbol{w_i} \times \boldsymbol{r}$.

A recent addition to the ICFD solver is the possibility to use periodic boundary conditions using the keyword *ICFD_BOUNDARY_PERIODIC to take advantage of repeating patterns in the flow. In this case, a third of the model can be defined and a periodicity condition applied on the two surfaces for the two variables velocity and pressure. The constraint system which is build is shown on Figure 2. Non-conforming meshes are possible, but it is recommended to use the same mesh on the two periodic surfaces.

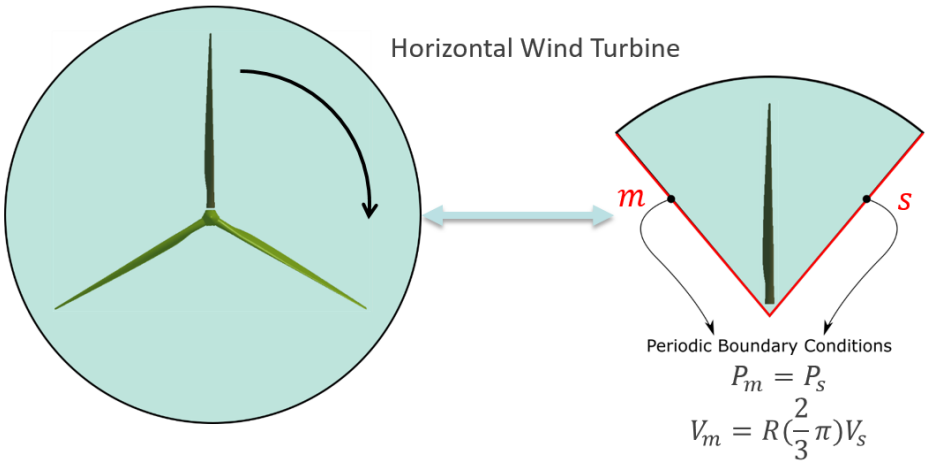

Figure 2 Periodic boundary condition. While the pressure degrees-of-freedom take on the same values, the fluid velocity degrees-of-freedom are constrained through a linear transformation with the rotation matrix R.

Finally, sliding mesh is a technique frequently used in turbomachinery or in similar settings involving a rotating structure. It consists in having a domain of the CFD mesh that follows the movement of the structure while the rest of the mesh remains static. For the ICFD solver, this is again handled by a constraint based method using *ICFD_BOUNDARY_PERIODIC. Two separate volume meshes must be defined, one of which will be allowed to move. The master surface then seeks an intersection face from the slave part and sets up the corresponding constraint as shown in Figure 3. Currently, the assembly of this constraint system is time consuming and potential improvements are being investigated.

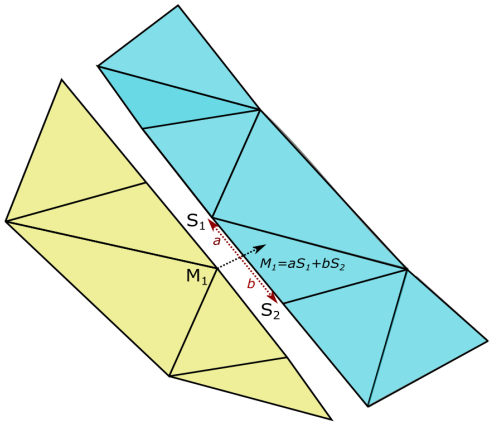

Figure 3 New constraint generated. The node normal from the master surface is used to find an intersection with the faces from the slave surface

Due to limited computation resource availability, the four configurations were not allowed to run for a period long enough to fully guarantee that a steady state has been reached. However, from the available results, some preliminary conclusions can be drawn. Figure 4 offers a comparison of the velocity profiles immediately after the wake for the non-inertial and periodic cases. The results seem to be in good agreement and the velocity seems to be at its highest magnitude at the mid-section of the blades. This is further confirmed by Figure 5 which offers a side view of the velocity profile. An important acceleration over the airfoil's upper camber can be observed. Figure 6 offers a comparison of the surface average pressure along the airfoil at this mid-section area. Again, good agreement is achieved between the periodic and the full 3D cases. Interestingly, it can be observed that the lower camber seems to have an important contribution to the total pressure forces acting on the airfoil which departs from the conventional behavior of airflow around an airfoil where the upper camber is usually the biggest contributor to lift, at least during the normal angle of attack range.

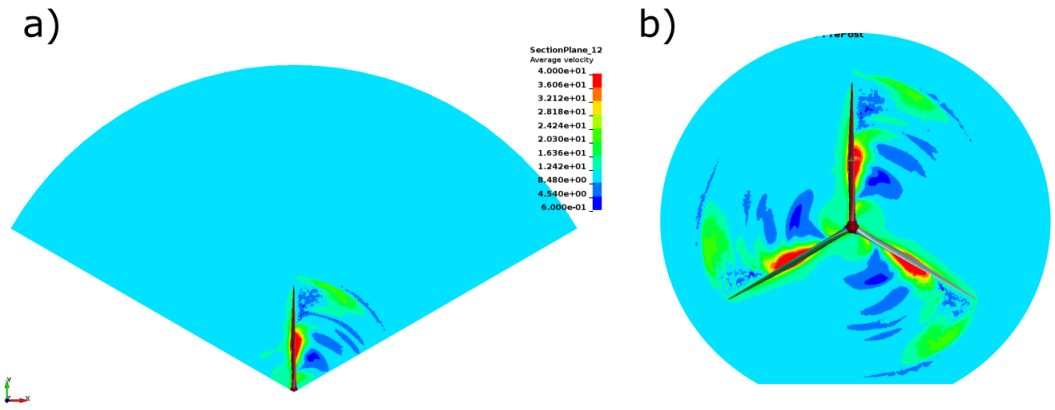

Figure 4 a) Periodic case and b) Full 3D case. Average velocity profile using a section plane in the immediate wake of the wind turbine

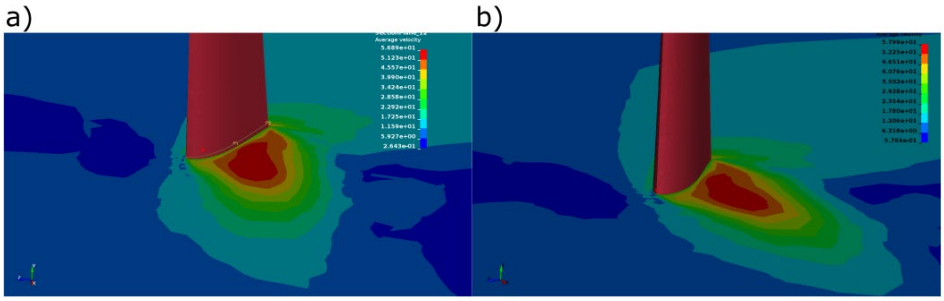

Figure 5 a) 3D case and b) Periodic case. Average velocity profile on a Section Plane at Y=30m

Finally, Figure 7 shows the torque acting on a blade for the four scenarios. Overall, the results are all in good agreement, the periodic and full 3D non inertial cases offer a very good match but also the sliding mesh case matches the mesh displacement case. The main difference are those peaks of pressure which are typically associated with a remeshing event. Usually, the pressure recovers after a few timesteps, but it can sometimes lead to some instabilities, especially in highly nonlinear FSI cases, thus prompting the user to choose his remeshing frequency with great care. This serves as a perfect highlighter to the benefits and comfort that sliding mesh capabilities can bring.

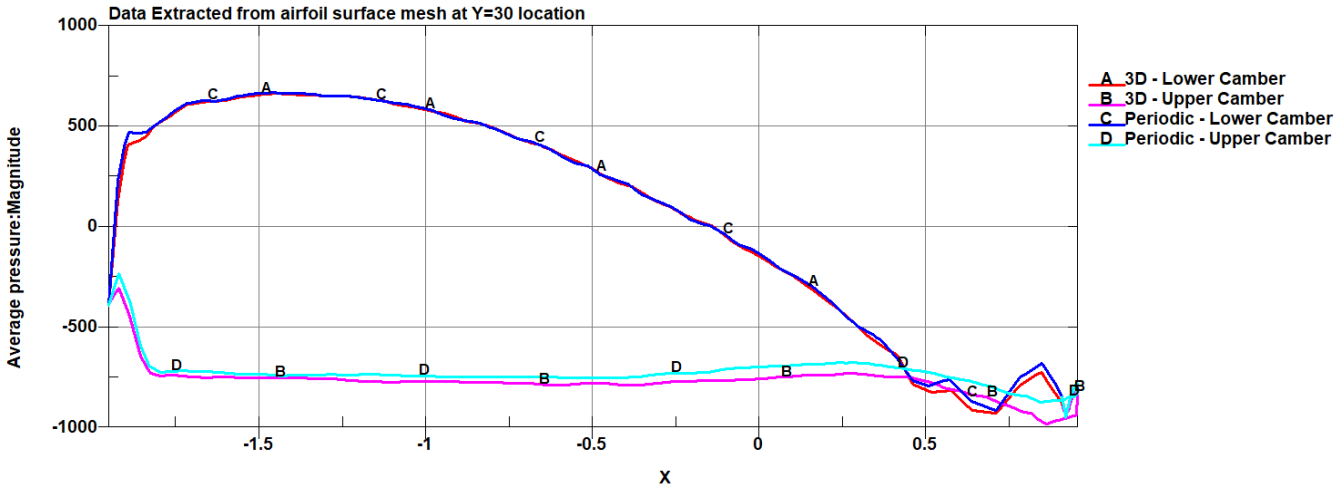

Figure 6 Average pressure of the surface of the airfoil at Y=30

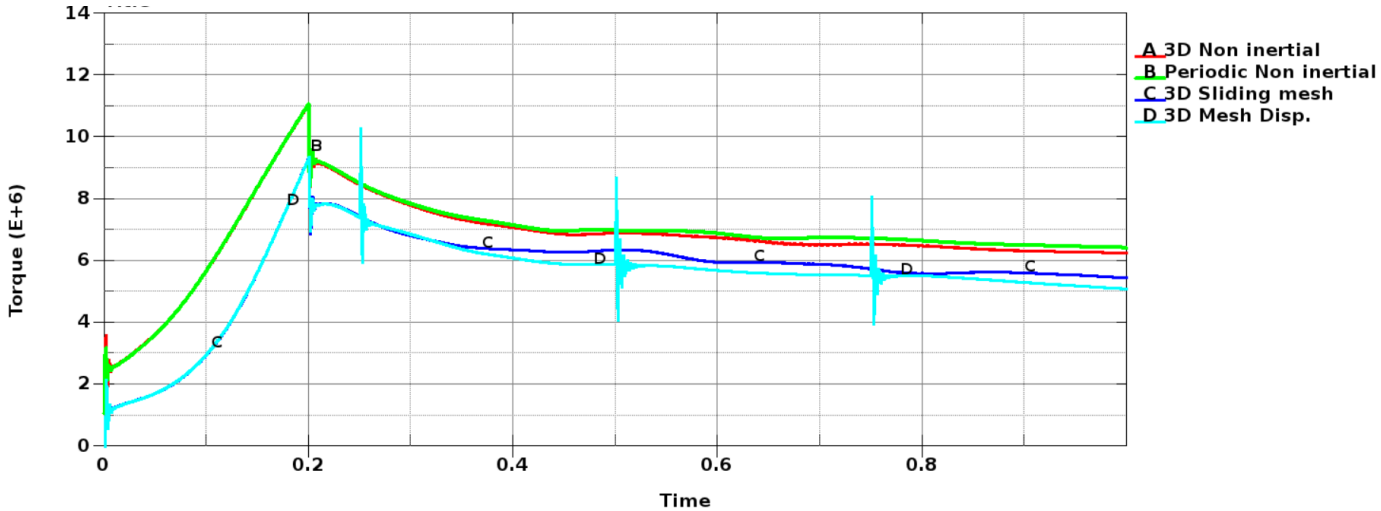

Figure 7 Evolution of the Torque acting on one blade in the first second for the four configurations

Blood pump for Medical device

A key step in the development of medical devices is the testing phase. Regulatory agencies like the Food and Drug Administration require extensive laboratory testing and a long, tedious and expensive clinical trial process before a device is approved for clinical use. In an effort to optimize this process, the industry and the regulatory agencies are looking at numerical methods as an additional tool that could potentially reduce the time of product development, animal testing and cost.

The first critical step is to increase the confidence, reliability and robustness of numerical techniques. The FDA is actively working on this subject by designing laboratory experiments that could be used to evaluate the solution accuracy provided by computational methods launching the Critical Path Initiative (CPI) [5] program. The aim of the program is to standardize the use of computational simulation on the design of the blood-contacting medical devices and analysis of the ratio of hemolysis in them. The goal of this project is to establish the guidelines for applying Computational Fluid Dynamics (CFD) techniques on the evaluation and the optimization of the medical devices.

Among the benchmark proposed ([6]) is the analysis of the flow in a simplified centrifugal blood pump which has been the subject of investigations using the ICFD solver in Huang [7].

The geometry of the FDA proposed simplified centrifugal pump is shown in Figure 4. The flow enters the chamber through a curved tube with diameter 12 mm. The diameter of the inner chamber of the housing is 60 mm and the thickness is 9 mm. The rotor inside the chamber has a diameter of 52 mm and 4 mm thick, along with four 3 mm thick straight blades. The chamber is connected with a throat at its outlet, followed by a diffuser to the outlet tube with diameter 12 mm. The flowrate is Q = 6 L/min and the rotational speed 3500 RPM.

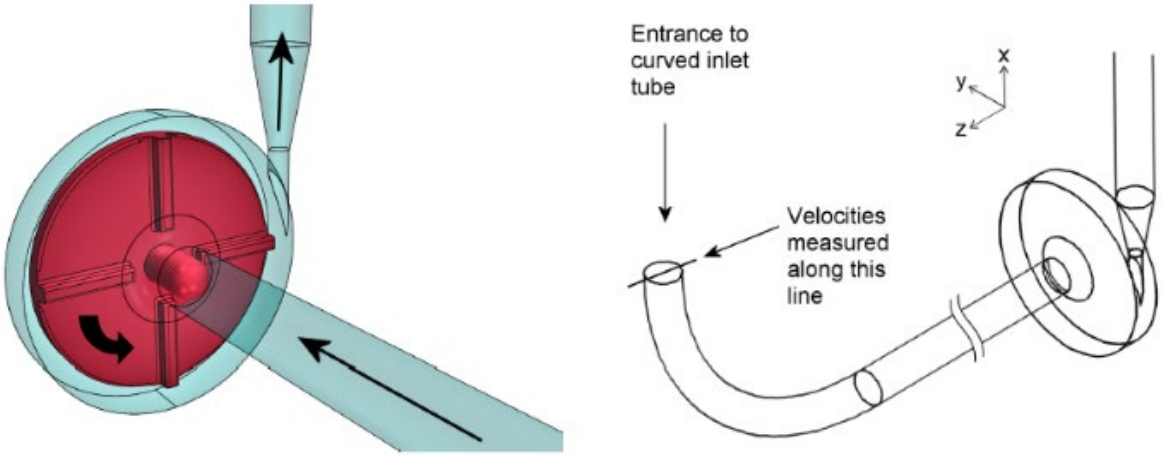

Figure 8 Pump geometry and flow direction in the blood pump (left), and inlet location where the velocity is measured in experiments and where the velocity profile is prescribed in the simulations (right)

This time, the LES Wall-Adapting Local Eddy-viscosity (WALE) [8] turbulence model is employed, and the total model size is around 1 Million elements. Two approaches, one using a non-inertial reference frame, the other using the sliding mesh technique are compared.

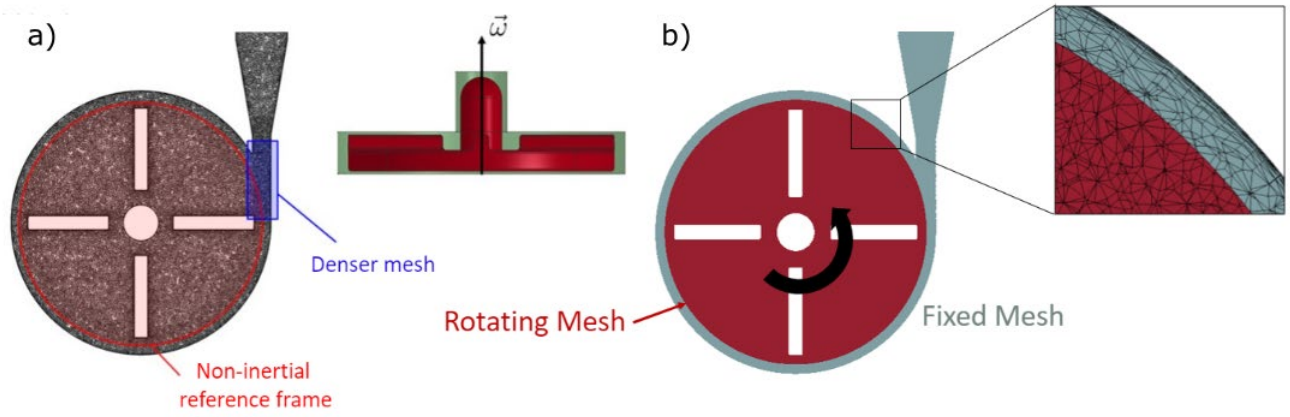

Figure 9 a) Non inertial and b) sliding mesh configurations for the blood pump

The pressure difference across the pump obtained by the experiment and the simulations are listed in Table 2 with both cases being in close agreement.

	Pressure (mmHg)
Experiment [9]	272.38
Non inertial	282.40
Sliding	283.54

The other quantities of interest are the velocity profiles in the pump chamber and diffuser compared with experimental measurements. The velocity profiles between blades are both in accordance with experiments. In the outlet diffuser, the non-inertial case predicts the detached jet leaning more against the outer wall and the velocity magnitude appears to be larger than experiments. The phenomenon may be due to the usage of the non-inertial reference frame approximation since similar velocity distribution in the diffuser can also be observed in most of the other numerical results that use non-inertial reference frame [9]. To confirm this observation, the sliding mesh result offers a better overall profile.

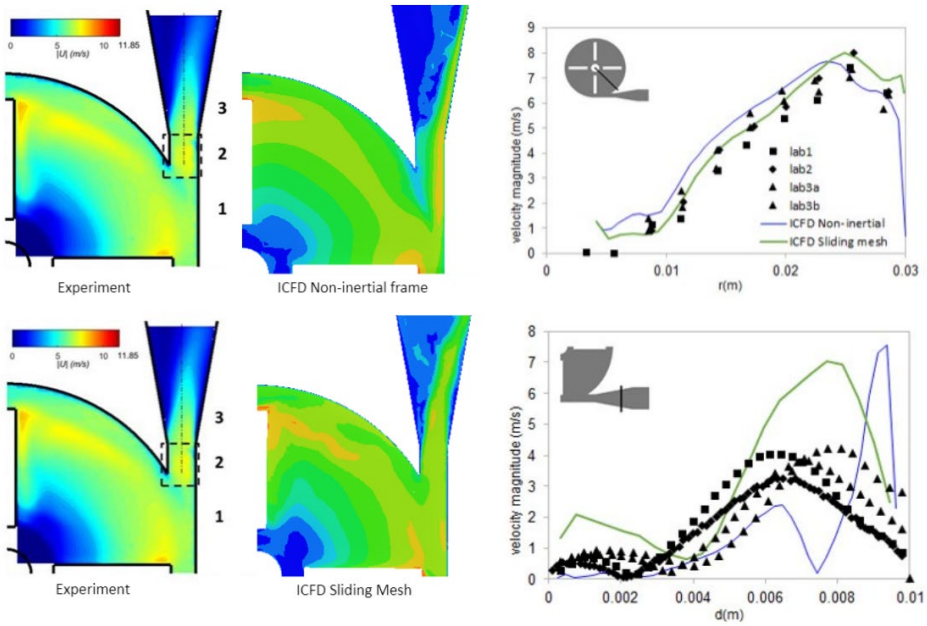

Figure 10 Results and comparisons of velocity profiles in the non-inertial reference frame and sliding mesh configurations

Conclusion

The different methods for solving rotating machinery problems using the ICFD solver have been presented. Two new capabilities have been introduced i.e periodic boundary conditions and sliding mesh. The two analyses conducted are encouraging and tend to offer some confidence as to the validity of the implementation. However, several challenges remain chiefly the handling of the constraint matrix which is time consuming and for which more development is required. Alternative solving methods are also investigated.

Finally it is important to note that, for the scope of this work, the blades have been left rigid, but the ICFD solver specializes in fluid structure interaction and it would be interesting to see the effect of flexible blades on the resulting torque. This will probably be part of a subsequent analysis. Overset and immersed FSI are also two numerical methods which are currently under development and investigation. When they become available, similar testing will be provided to complete the suite of results and cases made available to the users who wish to become familiar with the ICFD solver.

References

[1] Chorin AJ (1968).” Numerical Solution of the Navier- Stokes Equations. Mathematics of Computation”, 22(104):745{762.
[2] Temam R (1969). “On the Approximation of the Solution of Navier-Stokes Equations by the Fractional Steps Method II”. Archive for Rational Mechanics and Analysis, 32:377{385.
[3] Codina R (2000). “Stabilization of incompressibility and convection through orthogonal sub-scales in finite element methods”. Computer Methods in Applied Mechanics and Engineering, 190(13-14):1579{1599
[4] Bazilevs Y (2011). “3D simulation of wind turbine rotors at full scale. Part I: Geometry modeling and aerodynamics”. International Journal for Numerical Methods in Fluids 65(1-3):207 – 235
[5] FDA Critical Path Initiative (CPI), 2016. https://www.fda.gov/scienceresearch/specialtopics/criticalpathinitiative/default.htm
[6] FDAs \Critical Path" Computational Fluid Dynamics (CFD)/Blood Damage Project: Computational Round Robin problems, 2004. https://nciphub.org/wiki/FDA CFD
[7] Huang, CJ (2019). “On the performance and accuracy of PFEM-2 in the solution of biomedical benchmarks”. Computational Particle Mechanics volume 7, pages121–138(2020).
[8] Nicoud F, Ducros F (1999).” Subgrid-Scale Stress Modelling Based on the Square of the Velocity Gradient Tensor Flow”. Turbulence and Combustion, 62(3):183{200}.
[9] Malinauskas RA (2017).” FDA benchmark medical device flow models for CFD validation”. ASAIO Journal, 63(2):150{160.